MANSOURA JOURNAL OF CHEMISTRY
Official Journal of Faculty of Science, Mansoura University, Egypt
E-mail: scimag@mans.edu.eg ISSN: 2974-4938

Crystallization behavior of aluminum fluorosilicate glass systems doped with Niobium oxide.

A.M. Elsherbeny[a], A.M. Abdelghany[b], S.M. Ghorab[c], R.M. Shalaby[a]

[a]*Metal Physics Laboratory, Physics Department, Faculty of Science, Mansoura University, Mansoura, Egypt*

[b]*Spectroscopy Department, Physics Research Institute, National Research Centre, 33 Elbehouth St., Dokki, 123111, Giza, Egypt*

[c]*Department of Dental Biomaterials, Faculty of Dentistry, Mansoura University, Mansoura, Egypt*

**** Correspondence to:** amira_elsherbeny@mans.edu.eg, 01550586004*

Received:20/5/2025
Accepted:28/5/2025

Abstract: The present study investigates the crystallization behavior of aluminum fluorosilicate glass systems doped with Nb_2O_5 (0, 5, and 10 mol%) within the composition $45SiO_2–15Al_2O_3–10CaF_2–15Na_2O–5NaF–(10−x)SrO–xNb_2O_5$. Through comprehensive analyses using XRD, FTIR, SEM, and physical parameter measurements, the dual role of Nb_2O_5 as a nucleating agent and network modifier was elucidated. Results demonstrate that increasing Nb_2O_5 content significantly enhances crystallization, leading to the formation of niobium-rich phases such as $NaNbO_3$ while reducing the amorphous fraction. FTIR deconvolution revealed the incorporation of Nb^{5+} into the glass network, which promotes polymerization and modifies Al-O coordination. Theoretical density calculations exceeded experimental values due to microvoids and structural distortions induced by Nb_2O_5, highlighting the material's complex microstructure. SEM micrographs confirmed the progressive increase in crystallite density and size with higher Nb_2O_5 concentrations, transitioning from isolated crystallites to an interconnected crystalline network. The study underscores Nb_2O_5's ability to stabilize the glass network while driving crystallization, offering valuable insights for designing tailored glass-ceramics with controlled microstructures. These findings have significant implications for optical and engineering applications, where precise manipulation of crystallization behavior is critical for optimizing mechanical, thermal, and functional properties.

Keywords: Fluorosilicate glass; crystallization; glass-ceramic; Nb_2O_5.

1. Introduction

Fluorosilicate glasses have garnered significant attention in materials science due to their unique combination of optical, mechanical, and thermal properties, making them suitable for applications in photonics, laser hosts, and radiation shielding [1-3]. The compositional flexibility of these glasses allows for tailoring their properties by modifying the glass network through the incorporation of various oxides and fluorides. The system $45SiO_2–15Al_2O_3–10CaF_2–15Na_2O–5NaF–(10−x)SrO–xNb_2O_5$ (x = 0, 5, 10 mol%) presents an intriguing opportunity to study the interplay between network formers, modifiers, and intermediate oxides in a fluorine-rich environment, with particular implications for crystallization behavior—a critical factor in glass-ceramic development [4].

The SiO_2 (silica) serves as the primary glass former, establishing a stable tetrahedral network that ensures structural integrity. Al_2O_3 (alumina) acts as an intermediate oxide, enhancing chemical durability and thermal stability by occupying network-forming or modifying roles depending on composition. In fluorosilicate glasses, Al_2O_3 also influences crystallization kinetics by stabilizing the glass network or participating in phase separation, which can promote or inhibit devitrification [5, 6].

The addition of CaF_2 and NaF introduces fluoride ions, which lower melting temperatures, reduce viscosity, and improve optical transparency by breaking Si–O–Si bonds. However, fluorine content also affects crystallization behavior, as fluoride phases (e.g., CaF_2 or NaF crystals) may precipitate during heat treatment, influencing the final glass-ceramic microstructure [7]. Meanwhile, Na_2O acts as a network modifier, facilitating the depolymerization of the silicate network and enhancing ion mobility, which can alter phase separation and nucleation rates.

The substitution of SrO with Nb_2O_5 introduces an interesting dynamic. SrO (strontium oxide) typically behaves as a modifier, while Nb_2O_5 (niobium pentoxide) can act as an intermediate or conditional glass former, potentially enhancing refractive index, mechanical strength, and nonlinear optical properties. Niobium is also known to influence crystallization mechanisms, either by forming Nb-rich crystalline phases (e.g., $NaNbO_3$) or by suppressing crystallization due to its high field strength, which increases glass network stability [8-10].

Understanding the crystallization behavior of aluminum fluorosilicate glasses is crucial for designing glass-ceramics with controlled microstructures and tailored properties [11, 12]. The presence of Al_2O_3 and fluorine modifies phase separation tendencies, nucleation rates, and crystal growth, impacting mechanical strength, optical transparency, and thermal expansion. By systematically varying Nb_2O_5 content (x = 0, 5, 10 mol%), this study aims to investigate how niobium incorporation affects glass stability against crystallization and identify the dominant crystalline phases formed during heat treatment. Moreover, to correlate structural changes with crystallization trends.

This work provides fundamental insights into the composition structure crystallization relationship in fluorosilicate glasses, supporting the development of advanced glass-ceramics for optical, biomedical, and engineering applications. The choice of 0, 5, and 10 mol% Nb_2O_5 substitution represents a systematic investigation method that allows for a gradual and controlled modification of the glass network.

2. Materials and Methods

2.1. Glass preparation and crystallization

Glass samples of composition $45SiO_2$- $15Al_2O_3$- $10CaF_2$- $15Na_2O$- 5NaF- (10-*x*) SrO- *x*Nb_2O_5, where x=0, 5, 10 mol%, were previously synthesized and studied for their structural radiation shielding ability [4]. Analytical grade chemicals of Sodium carbonate and strontium carbonate supplied by Sigma Aldrich Co. are used to obtain sodium and strontium oxides. Silicon oxide and Niobium oxide supplied by Sigma Aldrich Co. was used as received. Aluminum oxide supplied by Lenksses Co. was used as received. Calcium and sodium fluorides from Membai Co..The two-step heat treatment process (nucleation followed by crystallization) for the studied glasses involves controlled thermal steps to induce crystal formation while maintaining structural stability. Nucleation is typically carried out near the glass transition temperature (Tg) to promote the formation of stable crystal nuclei without excessive growth. For this composition, a suitable nucleation temperature range is 560–580 °C for 1–2 hours based on a glass composition, allowing homogeneous distribution of nucleation sites, particularly for fluoride phases CaF_2, and potential Nb_2O_5-related clusters in Nb-containing glasses. The subsequent crystallization step is performed at a higher temperature (between 680–720°C for 1–3 hours, where the nuclei grow into well-defined crystalline phases.

2.2. Experimental Techniques

The X-ray diffraction (XRD) patterns of the prepared films were collected using PANalytical X'pert Pro MPD (with wavelength λ = 1.5406 Å, Cu-Kα radiation, and operating voltage 35 kV) in the 2Θ range (5–70°) in a continuous mode. FT-IR spectra measurements were carried out using a Bruker FT-IR spectrometer (Invenio S, Germany). The spectral resolution was 4 cm^{-1}, scan number was 64 within the wavenumber range of 4000–400 cm^{-1} was applied to the collection of ATR spectra. Scanning electron microscopy (QUANTA FEG 250 FE-SEM) was employed to analyze the surfaces of the specimens, their exact structures, crystalline structure, and materials composing the specimens.

The study involved the determination of several fundamental physical properties through both experimental measurements and theoretical calculations. Key parameters investigated included experimental and theoretical density, molar volume, and packing density to characterize the glass structure. Additional derived properties comprised free volume, average molecular weight, and ion concentration, which provide insights into the material's compactness and ionic distribution. Further analysis included polaron radius and inter-nuclear distance to assess electron localization effects and cation spacing, while field strength was evaluated to understand modifier ion influences. Finally, oxygen packing density was calculated to examine the oxygen ion arrangement within the glass network. Together, these parameters offer a comprehensive understanding of the glass system's structural and electronic characteristics. The parameters discussed in this study can be mathematically represented through the following fundamental equations [13-15]:

Theoretical density

$$\rho_{theo} = \frac{\sum_i (x_i M_i)}{V_m} \quad (1)$$

x_i is the mole fraction
M_i is the molecular weight of component i
V_m is the molar volume

molar volume

$$V_m = \frac{M_{avg}}{\rho} \quad (2)$$

M_{avg} is the average molecular weight of glass

Packing Density

$$V_t = \frac{\sum_i (x_i V_i)}{V_m} \quad (3)$$

V_i is the ionic volume of component i

Free Volume

$$V_f = V_m - \sum_i (x_i V_i) \quad (4)$$

Average Molecular weight

$$M_{avg} = \sum_i (x_i M_i) \quad (5)$$

Ion concentration

$$N = \frac{x N_A \rho}{M_{avg}} \quad (6)$$

Polaron radius

$$r_p = \frac{1}{2}\left(\frac{\pi}{6N}\right)^{1/3} \quad (7)$$

Field strength

$$F = \frac{Z}{r^2} \quad (8)$$

Z is the cation charge
r is the ionic radius of the cation

Oxygen packing density

$$OPD = \frac{Total\ oxygen\ atoms\ per\ formula\ unit \times \rho}{M_{avg}} \quad (9)$$

3. Results and Discussion

3.1. FTIR analysis of studied glass ceramics

Figure (1) presents FTIR spectra of heat-treated glass-ceramics in the system $45SiO_2$–$15Al_2O_3$–$10CaF_2$–$15Na_2O$–$5NaF$–$(10-x)SrO$–xNb_2O_5 (x = 0, 5, 10 mol%). The spectra maintain the characteristic bands observed in the previously reported glass [4], but with altered intensities and FWHM values. Four distinct features are visible: a medium-intensity sharp band at 455 cm^{-1}, a broad peak centered at 700 cm^{-1} with a shoulder at 590 cm^{-1} on its descending slope, and an intense broad peak at 970 cm^{-1}. No additional absorption bands are detected at higher wavenumbers. These spectral features can be assigned as follows: 455 cm^{-1} (Si-O-Si bending), 590 cm^{-1} (Nb-O stretching in NbO_6 octahedra), 700 cm^{-1} (Si-O-Al bridging vibrations), and 970 cm^{-1} (Si-O stretching in Q^2 and Q^3 units) [16-18].

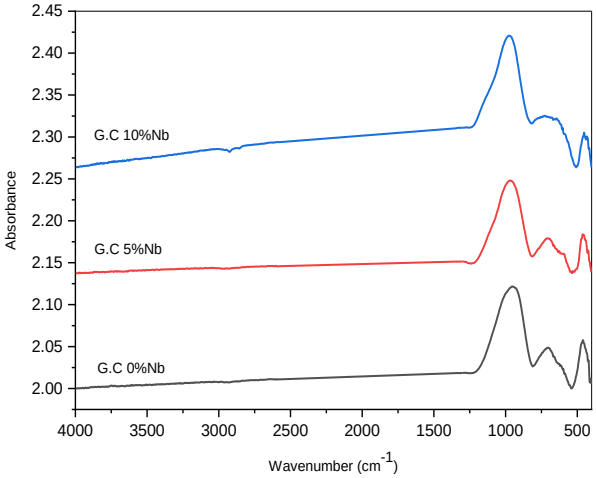

Figure (1) FTIR spectra of the studied samples

Deconvolution analysis was employed to quantify structural units (Al-O coordination, Q^2 and Q^3 silicate species) and elucidate the structural role of Nb_2O_5 in the glass-ceramic samples. The spectral components were separated using Gaussian fitting to resolve overlapping bands in the FTIR spectra [19, 20]. This analysis revealed changes in the relative proportions of different structural units as a function of Nb_2O_5 content, particularly highlighting the progressive incorporation of Nb^{5+} ions into the glass network. The deconvolution results, presented in Table 1, show that increasing Nb_2O_5 concentration (0 to 10 mol%) leads to: (1) a decrease in the relative proportion of Al-O units, suggesting that Nb^{5+} partially substitutes for Al^{3+} in tetrahedral sites; (2) an increase in Q^3/Q^2 ratio, indicating network polymerization; and (3) the emergence of new bands associated with Nb-O vibrations in both NbO_6 octahedra and NbO_4 tetrahedra, confirming the dual structural role of niobium as both network former and modifier. These structural changes correlate with the enhanced crystallization behavior observed in the XRD patterns. Figures (2:a, b, C) show the deconvoluted spectral data of the studied glasses.

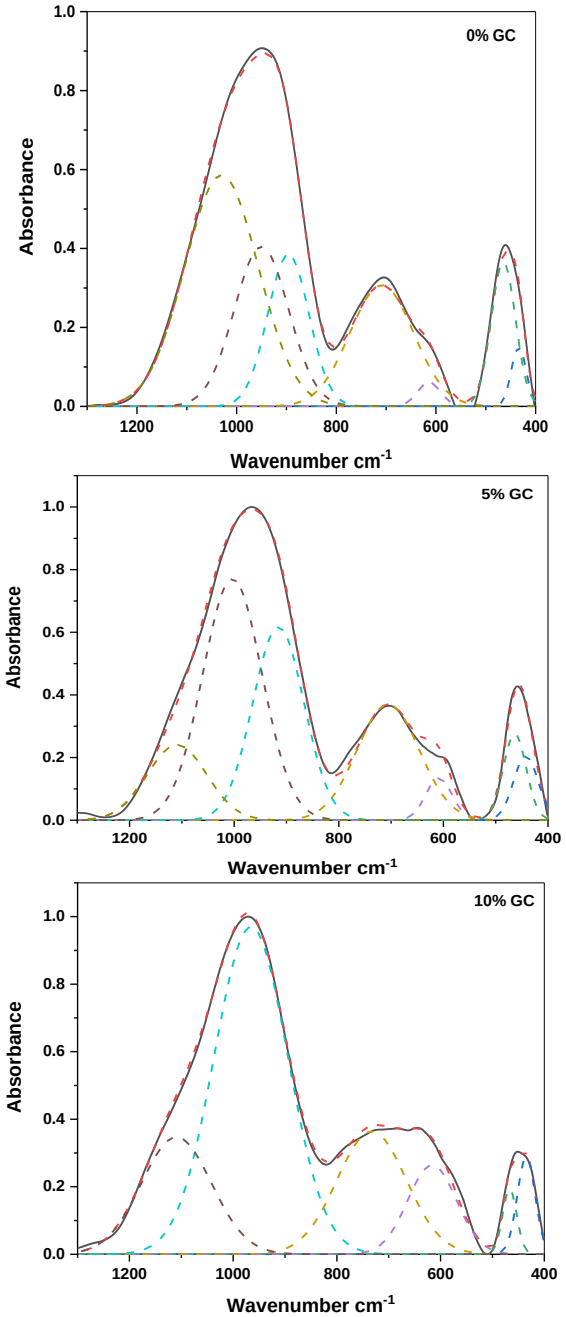

Figures (2:a, b, C) deconvoluted spectral data of the studied glasses.

Table (1) Deconvoluted data of studied samples

Sample	Center	Relative area	Q_1	Q_2	Q_3
GC 0% Nb	896 950 1030	0.231 0.260 0.508	0.231	0.2601 0.5084	___
GC 5% Nb	915 1003 1109	0.3456 0.4983 0.1559	0.345	0.4983	0.1559
GC 10% Nb	965 1109	0.2613 0.7386	___	0.2613	0.7386

3.2. X-ray diffraction (XRD)

Figure (3) reveals the X-ray diffraction pattern of the heat-treated samples. The produced pattern shows presence of multiple crystal peaks superimposed over an amorphous hump based on glass composition. Base glass shows broad hump centered at about 29° with several small peaks at about 21.5, 23, 26, 27, 28,29.5, 31,38, 39 and 45°.

The broad hump centered at $2\theta \approx 29°$ indicates that a significant portion of the material remains in the glassy (amorphous) state after heat treatment while the distinct peaks at 2θ values of approximately 21.5°, 23°, 26°, 27°, 28°, 29.5°, 31°, 38°, 39°, and 45° suggest the presence of one or more crystalline phases. Phase analysis indicate presence of Sodium Aluminosilicate ($NaAlSiO_4$, nepheline) (Card No.: 01-076-1858) [21] with major peaks at 21.8°, 23.1°, 27.2°, 29.7°, 30.9°, 38.4°, Strontium Aluminosilicate ($SrAl_2Si_2O_8$) (Card No.: 01-070-1862) [22] with major peaks at 22.1°, 23.9°, 27.0°, 27.9°, 31.2°, Sodium Calcium Aluminosilicate ($Na_2Ca_2Si_3O_9$) (card No.: 01-077-0386) [23] with a major peaks at 27.5°, 29.4°, 30.1°, 31.4°, 39.2° and with some residual of Calcium Fluoride (CaF_2, fluorite) (Card No.: 00-004-0864) [24] with a key peaks 28.3°, 47.0°, 55.6° and Sodium Fluoride (NaF) (Card No.: 00-004-0793) [25] with a Key peaks: 38.5°, 44.6°.

The relatively small intensity of the crystalline peaks compared to the amorphous hump suggests either a low volume fraction of crystals or nanocrystalline phases embedded in the glassy matrix.

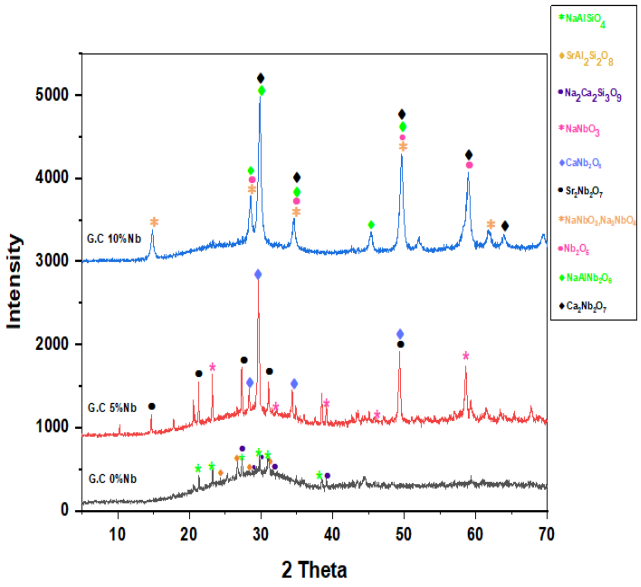

Figure (3) XRD pattern of the studied glass-ceramic

The addition of 5% Nb_2O_5 at the expense of SrO has significantly altered the crystallization behavior of the studied glass system. The new composition ($45SiO_2–15Al_2O_3–10CaF_2–15Na_2O–5NaF–5SrO- 5Nb_2O_5$) shows a more extensively crystallized material, as evidenced by the higher intensity peaks and reduced amorphous background. The small amorphous hump at ~29° indicates that most of the glass has crystallized, unlike the previous sample where a significant portion remained amorphous while the peaks at 15°, 18°, 21°, 22°, 24°, 27°, 28°, 30°, 32°, 35°, 39°, 50°, 51°, and 60° 2θ suggest multiple crystalline phases have formed including Sodium Niobate ($NaNbO_3$) (Card No.: 01-073-0803) with a Key peaks: 22.7°, 32.4°, 39.9°, 46.5°, 57.8°, Calcium Niobate ($CaNb_2O_6$) (Card No.: 00-039-1392) with a Key peaks: 28.9°, 30.1°, 34.8°, 50.3°, Strontium Niobate ($Sr_2Nb_2O_7$) **(**Card No.: 01-070-0413) with a key peaks: 15.3°, 21.6°, 27.5°, 31.9°, 50.6°, in addition to some of the previously reported phases Sodium Aluminum Silicate Fluoride ($Na_3AlSiO_4F_2$), Sodium Calcium Silicate ($Na_2Ca_2Si_3O_9$), Calcium Fluoride (CaF_2).

The appearance of the low-angle peak at 15° 2θ is particularly noteworthy, as it often indicates the formation of layered structures or phases with large unit cells, which is consistent with complex niobium-containing compounds like $Sr_2Nb_2O_7$. The presence of Nb_2O_5 has acted as an effective nucleating agent, significantly enhancing the crystallization process in the studied glass system. Niobium compounds tend to form nucleation sites that promote the crystallization of other phases, explaining the increased number and intensity of diffraction peaks.

The further increase in Nb_2O_5 content to 10% (at the expense of SrO, presumably making the composition $45SiO_2–15Al_2O_3–10CaF_2–15Na_2O–5NaF–0SrO–10Nb_2O_5$) has led to an even more dramatic change in crystallization behavior. The almost complete disappearance of the amorphous hump indicates a highly crystallized material, while the reduced number of peaks with higher intensities suggests preferential growth of specific crystalline phases. Sodium Niobate ($NaNbO_3$), Sodium Niobium Oxide (Na_3NbO_4) (Card No.: 01-076-0977) [26] with a key peaks: 15.2°, 28.9°, 35.4°, 50.3°, 62.1°, Niobium Oxide (Nb_2O_5) **(**Card No.: 00-027-1003) [27] with a key peaks: 28.4°, 35.1°, 49.7°, 58.8° result from excess unreacted Nb_2O_5 that may be present due to its higher concentration, Sodium Aluminum Niobate ($NaAlNb_2O_6$) (Card No.: 00-044-0060) [28] with a key peaks: 28.3°, 29.6°, 35.3°, 46.2°, 50.5°, Calcium Niobium Oxide ($Ca_2Nb_2O_7$) (Card No.: 01-070-1690) with a key peaks: 28.7°, 35.2°, 49.9°, 59.1°, 64.3° and finally Calcium Fluoride (CaF_2).

The significant changes in the XRD pattern with increasing Nb_2O_5 content can be explained as Niobium oxide is a powerful nucleating agent that promotes crystallization. At 10% concentration, it has induced nearly complete crystallization of the glass, while the decrease in the number of diffraction peaks suggests that certain phases are preferentially growing at the expense of others, leading to a simpler phase assemblage dominated by niobium-containing compounds. With SrO now completely replaced by Nb_2O_5, strontium-containing phases have disappeared, and the system is dominated by sodium and calcium niobate phases. The increased peak intensities indicate larger crystal sizes or higher volume fractions of crystalline phases. The presence of fewer peaks with higher intensities might also suggest some preferential orientation of the crystals, particularly for the layered niobium-containing phases.

This evolution in crystallization behavior demonstrates how Nb_2O_5 acts not only as a nucleating agent but also as a network modifier that fundamentally alters the structural organization of the glass-ceramic system. The complete crystallization and formation of predominantly niobium-containing phases suggest that the material has undergone a significant transformation from a glass-ceramic to an almost fully crystalline ceramic material.

In Nb-free glasses (x = 0), SrO and CaF_2 likely dominate crystallization, forming SrF_2 or silicate phases, while increasing Nb_2O_5 content (x = 5, 10 mol%) may induce the precipitation of Nb-rich crystalline phases (e.g., $NaNbO_3$) or suppress crystallization due to Nb's high field strength, requiring optimization of time-temperature parameters to balance phase purity and microstructure.

2.3. Scanning Electron Microscopy (SEM)

Figure (4) presents high-magnification electron micrographs of the investigated glass-ceramic samples. The images reveal nanocrystalline phases embedded within the amorphous glass matrix, with crystallite density and size progressively increasing with Nb_2O_5 content. In the niobium-free sample, sparse, isolated crystallites are observed, while the 5 mol% Nb_2O_5 sample displays a higher volume fraction of uniformly distributed crystallites. At 10 mol% Nb_2O_5, the microstructure is dominated by an interconnected crystalline network with minimal residual glass phase.

This microstructural evolution directly corresponds to the XRD findings, confirming Nb_2O_5's role as an effective nucleating agent. The transformation from predominantly amorphous to highly crystalline character is evidenced by the decreasing glass background in the micrographs, paralleling the diminishing amorphous hump in the diffraction patterns. The observed crystallites likely represent the niobium-rich phases identified by XRD, including sodium niobate and calcium niobium oxide compounds. This relationship between Nb_2O_5 concentration and crystallization behavior demonstrates how controlled additions of nucleating agents can be used to engineer the microstructure of glass-ceramics for specific applications.

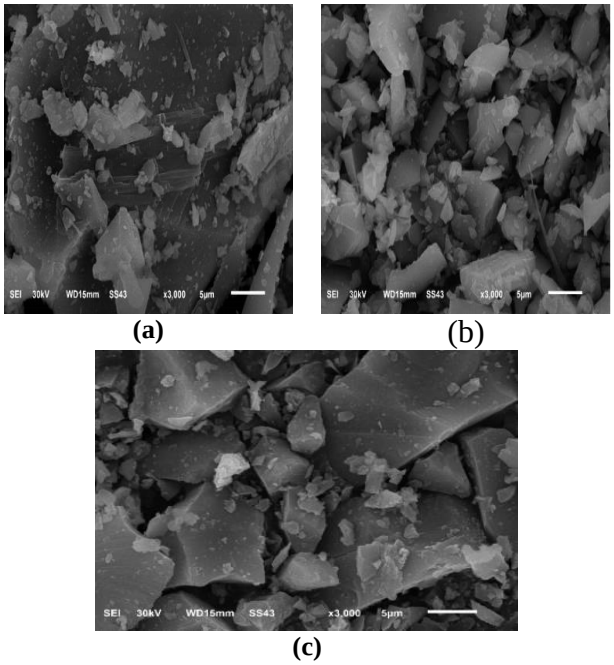

Figure (4) SEM of samples (a) GC-Nb0, (b) GC-Nb5, and (c) GC-Nb10.

2.4. Physical parameters

The higher values of theoretical density compared to experimental density in glass systems can be attributed to several factors. The theoretical calculation assumes an ideal, defect-free structure with perfect atomic packing and exact stoichiometric ratios, whereas real glasses contain microvoids, composition fluctuations, and residual stresses from processing that increase volume and reduce measured density. Additionally, experimental techniques like Archimedes' method are affected by surface roughness, bubble entrapment, and measurement uncertainties, further lowering the experimental values. In the specific case of Nb_2O_5-containing glasses, the high field strength of Nb^{5+} ions may distort the network structure, creating more open coordination geometries and increasing interatomic spacing despite the glass high molecular weight. Furthermore, rapid quenching during glass synthesis can trap excess free volume, while fluorine content may lead to volatilization-induced porosity. These combined effects—idealized theoretical assumptions versus real structural imperfections and measurement limitations—systematically result in theoretical density values exceeding their experimental counterparts, typically by 1-5% in oxide glasses, with larger discrepancies possible in systems containing heavy modifiers or flux additives. The difference serves as an important indicator of the glass's true microstructure relative to its idealized composition. All obtained data were summarized in Table 2.

Table (2) Calculated physical parameters

parameters	Glass Code		
	S1	S2	S3
Density gcm^{-3}±0.0002	2.667	2.664	2.628
Theoritical density gcm^{-3}	3.048	3.043	3.038
Molar volume (Vm) cm^3mol1±0.0001	26.957	30.032	33.529
Packing density (Pd)	0.529	0.518	0.503
Free volume (Vf)	12.686	14.472	16.680
Average mol.wt. (MAv)(g)	71.896	80.005	88.115
Ion concentration (N) (10^{+23} ions)	0.000	1.002	1.795
Polaron radius (r_p) (A°)	-	0.867	0.714
Inter-nuclear distance (r_i) (A°)	-	2.153	1.773
Field strength (F) 10+18 (g mol1cm^{-2})	-	3.532	5.211
Oxygen Packing density (OPd) 10^{+21}	1.320	1.200	1.070

2.5. O/N (oxygen per network-forming cation)

The oxygen per network-forming cation (O/N) ratio provides critical insights into the structural organization of these aluminum fluorosilicate glasses. For the composition containing 10 mol% Nb_2O_5 (with no SrO), we calculate an O/N ratio of 2.68, reflecting a highly polymerized network structure. This low ratio results from niobium's strong tendency to act as a network former, with Nb^{5+} ions incorporating into the glass matrix as [NbO_6] or [NbO_4] units that enhance three-dimensional connectivity. The intermediate composition (5 mol% Nb_2O_5 and 5 mol% SrO) shows a moderately higher O/N of 2.88, indicating a balance between network-forming (Nb_2O_5) and network-modifying (SrO) influences. In contrast, the SrO-rich (10 mol%) glass exhibits the highest O/N ratio of 3.04, characteristic of a significantly depolymerized structure with abundant non-bridging oxygens due to Sr^{2+}'s modifier role.

These calculated O/N values correlate remarkably well with the experimental observations from XRD and FTIR analyses. The decreasing O/N ratio with increasing Nb_2O_5 content explains the enhanced crystallization tendency observed in these glasses, as the more polymerized network provides favorable conditions for ordered phase formation. Conversely, the higher O/N values in SrO-containing compositions correspond to their greater network disruption and reduced crystallization propensity. The systematic variation in O/N ratios (from 2.68 to 3.04) across these compositions quantitatively demonstrates how strategic compositional adjustments can precisely control the glass network's degree of polymerization, offering a powerful tool for tailoring material properties for specific applications in optics, electronics, or glass-ceramic technologies. This approach provides a fundamental framework for understanding and predicting structure-property relationships in complex multi-component glass systems.

4. Conclusion

The systematic substitution of SrO with Nb_2O_5 in aluminum fluorosilicate glasses significantly alters their crystallization behavior and structural properties. Nb_2O_5 acts as an effective nucleating agent, inducing the formation of niobium-rich crystalline phases (e.g., $NaNbO_3$) and reducing amorphous content, as confirmed by XRD and SEM. FTIR analysis reveals Nb^{5+} integration into the network, increasing polymerization and modifying Al-O coordination. Physical parameter calculations highlight the impact of Nb's high field strength on density and free volume, with theoretical values surpassing experimental results due to structural imperfections. These findings underscore Nb_2O_5's dual functionality—enhancing network stability while promoting crystallization—enabling the design of advanced glass-ceramics with optimized mechanical, optical, and thermal properties for targeted applications. The study provides a foundation for further exploration of Nb-doped fluorosilicate systems in materials science.

References

1. Li, P., Xu, X., Zhao, J., Awasthi, P., Qiao, X., Du, J., & Qian, G. (2022). Lanthanide doped fluorosilicate glass-ceramics: A review on experimental and theoretical progresses. *Journal of Rare Earths*, **40(2),** 169-192.
2. Gali, S., Arjun, A., & Premkumar, H. B. (2024). Zirconia toughened fluorosilicate glass-ceramics for dental prosthetic restorations. Materials Chemistry and Physics, 324, 129703.
3. Elsherbeny, A. M., Abdelghany, A. M., Ghorab, S. M., & Shalaby, R. M. (2025). Investigating the impact of Nb_2O_5 on structural and shielding properties of aluminum fluorosilicate glass systems. Radiation Physics and Chemistry, 235, 112824.
4. Wang, D., Zhang, Q., Chen, C., Su, M., Zhang, S., & Wei, W. (2021). Preparation and photoluminescence of $Tm^{3+}/Eu^{2+}/Eu^{3+}$ tri-doped fluorosilicate glass ceramics for warm WLED. Optical Materials, 118, 111253.
5. Weng, W., Wang, X., Tian, K., Liu, D., Shao, Y., Zhao, H., & Wang, P. (2024). C-band laser emission from Er^{3+}-doped fluorosilicate glass microspheres and its application in temperature

sensing. *Journal of Luminescence*, ***265,*** 120205.
6. Cormier, L. (2021). Glasses: aluminosilicates. Encyclopedia of materials: Technical Ceramics and glasses, 496-518.
7. Suresh, S., Narendrudu, T., Yusub, S., Kumar, A. S., Kumar, V. R., Veeraiah, N., & Rao, D. K. (2015). Influence of local structural disorders on spectroscopic properties of multi-component CaF_2-Bi_2O_3-P_2O_5-B_2O_3 glass ceramics with Cr_2O_3 as nucleating agent. Spectrochimica acta. Part A, Molecular and Biomolecular Spectroscopy, **153,** 281-288.
8. He, X. (2013). Oriented micro/nano-crystallization in silicate glasses under thermal or laser field for mastering optical non-linear optics in bulk (Doctoral dissertation, Université Paris Sud-Paris XI; Wuhan University of Technology).
9. Wang, L., Ma, Y., Yu, X., Alsaiari, N. S., Algarni, Z., & Amari, A. (2025). Transparent $NaNbO_3$ glass-ceramics for wastewater treatment utilizing piezocatalysis and photo-piezocatalysis. Ceramics International.
10. Al-Obiedy, A. N., & Al-Helli, A. H. (2025). A review of the state-of-the-art in improving piezoelectric properties. *Advances in Science and Technology. Research Journal*, **19(6),** 41-69.
11. Müller, R., Zanotto, E. D., & Fokin, V. M. (2000). Surface crystallization of silicate glasses: nucleation sites and kinetics. *Journal of non-crystalline solids*, *274*(1-3), 208-231.
12. Kilinc, E., Bell, A. M., Bingham, P. A., & Hand, R. J. (2021). Effects of composition and phase relations on mechanical properties and crystallization of silicate glasses. *Journal of the American Ceramic Society*, **104(8),** 3921-3946.
13. Abdelghany, A. M., El-Batal, H. A., EzzEl-Din, F. M., ElAlialy, N., Okasha, A., Atta, D., ... & Awad, W. (2024). Structural and gamma-ray attenuation of mixed former lead-free borophosphate glasses. Radiation Physics and Chemistry, **214,** 111276.
14. Madshal, M. A., El-Damrawi, G., Abdelghany, A. M., & Abdelghany, M. I. (2021). Structural studies and physical properties of Gd_2O_3-doped borate glass. *Journal of Materials Science: Materials in Electronics*, **32(11)**, 14642-14653.
15. Abdelghany, A. M., & Behairy, A. (2020). Optical parameters, antibacterial characteristics and structure correlation of copper ions in cadmium borate glasses. *Journal of Materials Research and Technology*, **9(5),** 10491-10497.
16. Karmakar, B., Kundu, P., & Dwivedi, R. N. (2001). IR spectra and their application for evaluating physical properties of fluorophosphate glasses. *Journal of non-crystalline solids*, **289(1-3)**, 155-162.
17. Zhang, S., Stamboulis, A., & Ni, W. (2019). The effect of boron substitution for aluminium on the microstructure of calcium fluoro-aluminosilicate glasses and glass-ceramics. *Journal of the European Ceramic Society*, **39(5)**, 1918-1924.
18. Baasner, A., Schmidt, B. C., Dupree, R., & Webb, S. L. (2014). Fluorine speciation as a function of composition in peralkaline and peraluminous Na_2O–CaO–Al_2O_3–SiO_2 glasses: a multinuclear NMR study. Geochimica et Cosmochimica Acta, **132,** 151-169.
19. Handke, M., Mozgawa, W., & Nocuń, M. (1994). Specific features of the IR spectra of silicate glasses. *Journal of molecular structure*, **325**, 129-136.
20. Dalby, K. N., & King, P. L. (2006). A new approach to determine and quantify structural units in silicate glasses using micro-reflectance Fourier-Transform infrared spectroscopy. American Mineralogist, **91(11-12),** 1783-1793.
21. Theerapapvisetpong, A. (2011). High temperature glass ceramic sealants from R_2O-RO-AI_2O_3-SiO_2 (Doctoral dissertation, Chulalongkorn University).
22. Soylu, A., Karaahmet, O., & Cicek, B. (2024). Exploring luminescence in transparent glass–ceramic coating: Study on Pr^{3+}/Dy^{3+} Co-doped SrO–Al_2O_3–SiO_2 glass–ceramic particles. Materials Chemistry and Physics, **318**, 129250.

23. e Silva, D. L. C., Araújo, M. S., Fungaro, D. A., & Mello-Castanho, S. (2024). Thermal evaluation of a Cs-loaded waste vitrification. *Brazilian Journal of Radiation Sciences*, *12*(4A (Suppl.)), e2646-e2646.
24. Shakooei, M., Shahidi, M. M., Abedi, A., & Mehrabani, M. (2024). Analyzing Optical Properties of Natural Fluorite Crystals: A Comprehensive Investigation.
25. Lumeau, J., Chamma, K., Glebova, L., & Glebov, L. B. (2014). X-ray diffraction study of NaF nano-crystals in photo-thermo-refractive glass. *Journal of non-crystalline solids*, **405**, 188-195.
26. Shanker, V., Samal, S. L., Pradhan, G. K., Narayana, C., & Ganguli, A. K. (2009). Nanocrystalline $NaNbO_3$ and $NaTaO_3$: Rietveld studies, Raman spectroscopy and dielectric properties. Solid State Sciences, **11(2)**, 562-569.
27. Kodama, R., Terada, Y., Nakai, I., Komaba, S., & Kumagai, N. (2006). Electrochemical and in situ XAFS-XRD investigation of Nb_2O_5 for rechargeable lithium batteries. *Journal of the Electrochemical Society*, **153(3),** A583.
28. Morais, L. A., Adán, C., Araujo, A. S., Guedes, A. P., & Marugán, J. (2017). Synthesis, characterization, and photonic efficiency of novel photocatalytic niobium oxide materials. Global Challenges, **1(9)**, 1700066.